Microbiology and Infectious Disease

Ebola Virus Sequesters IRF3 in Viral Inclusion Bodies to Evade Host Antiviral Immunity

Lin Zhu, Jing Jin, Tingting Wang, Yong Hu, Hainan Liu, Ting Gao, Qincai Dong, Yanwen Jin, Ping Li, Zijing Liu, Xuan Liu , Cheng Cao

Institute of Biotechnology, Academy of Military Medical Sciences, Beijing, 100850, China • Institute of Physical Science and Information Technology, Anhui University, Hefei, Anhui 230601, China

Reviewed Preprint

Published from the original preprint after peer review and assessment by eLife.

About eLife's process

Reviewed preprint posted
June 27, 2023 (this version)

Posted to bioRxiv
April 26, 2023

Sent for peer review
April 20, 2023

Abstract

Viral inclusion bodies (IBs) are commonly formed during the replication of Ebola virus (EBOV) in infected cells, but their role in viral immune evasion has rarely been explored. Here, we found that interferon regulatory factor 3 (IRF3), but not TANK-binding kinase 1 (TBK-1) or IκB kinase epsilon (IKKε), was recruited and sequestered in viral IBs when the cells were infected by EBOV transcription- and replication-competent virus-like particles (trVLPs). NP/VP35-induced IBs formation was critical for IRF3 recruitment and sequestration, probably through STING interaction. Consequently, the association of TBK1 and IRF3, which plays a vital role in type I interferon (IFN-I) induction, was blocked by EBOV trVLPs infection. Additionally, IRF3 phosphorylation and nuclear translocation induced by Sendai virus (SeV) or poly(I:C) stimulation were also suppressed by EBOV trVLPs. Furthermore, downregulation of STING significantly attenuated VP35-promoted IRF3 accumulation in IBs. Viral proteins by which IBs-like structures could be formed were demonstrated to be much more potent in IFN-I antagonism than the expression of the IFN-I antagonist VP35 only. These results suggested a novel immune evasion mechanism by which EBOV evades host innate immunity.

Impact statement

Ebola virus VP35 protein evades host antiviral immunity by interacting with STING to sequester IRF3 into inclusion bodies and inhibit type-I interferon production.

eLife assessment

This study explores how Ebola virus evades human immune responses. The study reports a potential new mechanism wherein Ebola virus traps human IRF3, a key transcription factor involved in immune signaling, into virus-produced "inclusion bodies." While overall the topic is **important** and the paper has many merits, readers should note that the reviewers identified some flaws in the experimentation, analyses, and description of methods, which means the strength of evidence is currently **incomplete**.

Introduction

Ebola virus disease is the deadliest infectious disease caused by infection with Ebola virus (EBOV), an enveloped, nonsegmented negative-sense RNA virus (Feldmann, Jones, Klenk, & Schnittler, 2003). The 19-kb viral genome comprises seven genes encoding the nucleoprotein (NP), virion protein 35 (VP35), VP40, glycoprotein (GP), VP30, VP24 and RNA-dependent RNA polymerase (L) (Mahanty & Bray, 2004). Inclusion bodies (IBs) formed in EBOV-infected cells are specialized intracellular compartments that serve as sites for EBOV replication and the generation of progeny viral RNPs (Hoenen et al., 2012; Nanbo, Watanabe, Halfmann, & Kawaoka, 2013). In IBs, the EBOV genome is replicated and transcribed by viral polymerase complexes (Misasi & Sullivan, 2014). VP35 serves as a cofactor of RNA-dependent RNA polymerase and contributes to viral replication by homo-oligomerization through a coiled-coil domain (Reid, Cardenas, & Basler, 2005), in addition to its recently discovered presence of phosphorylation and ubiquitination (van Tol et al., 2022; Zhu et al., 2020).

Innate interferon responses constitute the first lines of host defense against viral infection. Retinoic acid-inducible gene I (RIG-I)-like receptors, including RIG-I and melanoma differentiation-associated protein 5, play pivotal roles in the response to RNA virus infection. After the recognition of RNA virus infection, RIG-I is recruited to the mitochondrial antiviral adaptor protein (MAVS) through the caspase activation and recruitment domain. The activation of MAVS recruits multiple downstream signaling components to mitochondria, leading to the activation of inhibitor of κ-B kinase ε (IKKε) and TANK-binding kinase 1 (TBK1), which in turn phosphorylate IFN regulatory factor 3 (IRF3). Phosphorylated IRF3 forms a dimer that translocates to the nucleus, where it activates the transcription of type I interferon (IFN-I) genes (Fitzgerald et al., 2003; Liu et al., 2015).

To promote viral replication and persistence, viruses have evolved various strategies to evade or subvert host antiviral responses. For example, severe fever with thrombocytopenia syndrome virus (SFTSV) has developed a mechanism to evade host immune responses through the interaction between nonstructural proteins and IFN-I induction proteins, including TBK1, IRF3 and IRF7 (Hong et al., 2019; Lee & Shin, 2021; Ning et al., 2014; Wu et al., 2014), sequestering them inside SFTSV-induced cytoplasmic structures known as IBs. In addition to inhibiting IFN-I induction, SFTSV nonstructural proteins can hijack STAT1 and STAT2 in IBs to suppress IFN-I signaling (Ning et al., 2015). These studies highlight the role of viral IBs as virus-built “jails” that sequester some crucial host factors and interfere with the corresponding cellular processes.

EBOV uses various approaches to evade the host immune response, including antagonizing IFN production, inhibiting IFN signaling, and enhancing IFN resistance (Basler et al., 2000;

McCarthy et al., 2016; Reid et al., 2006). VP35 is an IFN-I inhibitor that antagonizes host innate immunity by interacting with TBK1 and IKKε (Basler et al., 2003; Prins, Cardenas, & Basler, 2009), suppressing RNA silencing and inhibiting dendritic cell maturation (Haasnoot et al., 2007; Yen, Mulder, Martinez, & Basler, 2014). Here, we report that viral IBs in EBOV trVLPs-infected cells appear to play a role in immune evasion by sequestering IRF3 into IBs and preventing the interaction of IRF3 with TBK1 and IKKε.

Results

IRF3 is hijacked into cytoplasmic IBs in EBOV transcription and replication-competent virus-like particles infected cells

When HepG2 cells were infected with EBOV transcription and replication-competent virus-like particles (trVLPs) (Hoenen, Watt, Mora, & Feldmann, 2014), which authentically model the complete virus life cycle, IBs with a unique structure and viral particles formed in the cytoplasm (Fig. 1 – figure supplement 1A-B). Surprisingly, we found that a substantial percentage of endogenous IRF3 was trapped in viral IBs in EBOV trVLP-infected cells with large IBs (Fig. 1A), while no detectable TBK1 or IKKε, the essential upstream components of IRF3 signaling (Fitzgerald et al., 2003), was sequestered in the viral IBs (Fig. 1B and 1C). These results suggested that IRF3 was specifically compartmentalized in viral IBs, and this compartmentalization spatially isolated IRF3 from its upstream activators TBK1 and IKKε.

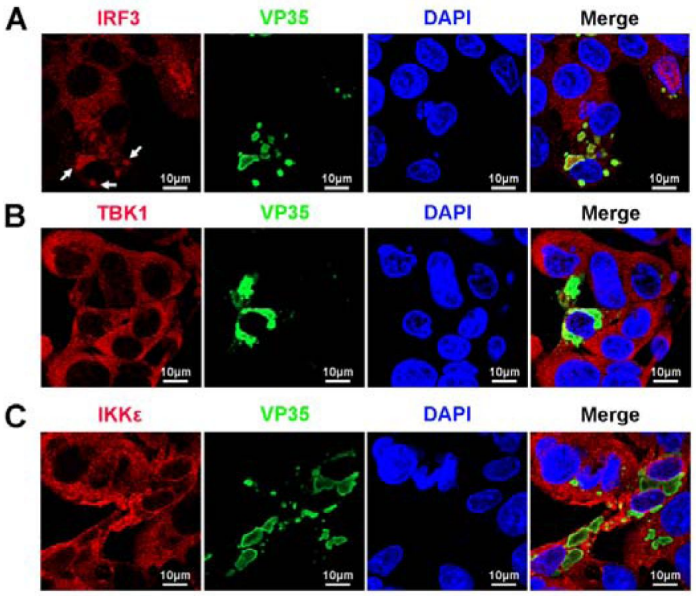

Fig. 1

IRF3, but not TBK1 and IKKε, is sequestered into viral inclusion bodies (IBs) upon EBOV trVLPs infection.

(A), HepG2 cells transfected with the EBOV minigenome (p0) were immunostained with anti-IRF3 (red) and anti-VP35 (green) antibodies. White arrows: IRF3 in IBs. (B and C), HepG2 cells transfected with the EBOV minigenome (p0) were immunostained with anti-TBK1 (red in (B)) or anti-IKKε (red in (C)) and anti-VP35 (green in (B and C)) antibodies. Nuclei were stained with DAPI (blue), and images were obtained using a Zeiss LSM 800 Meta confocal microscope. Scale bar, 10 μm.

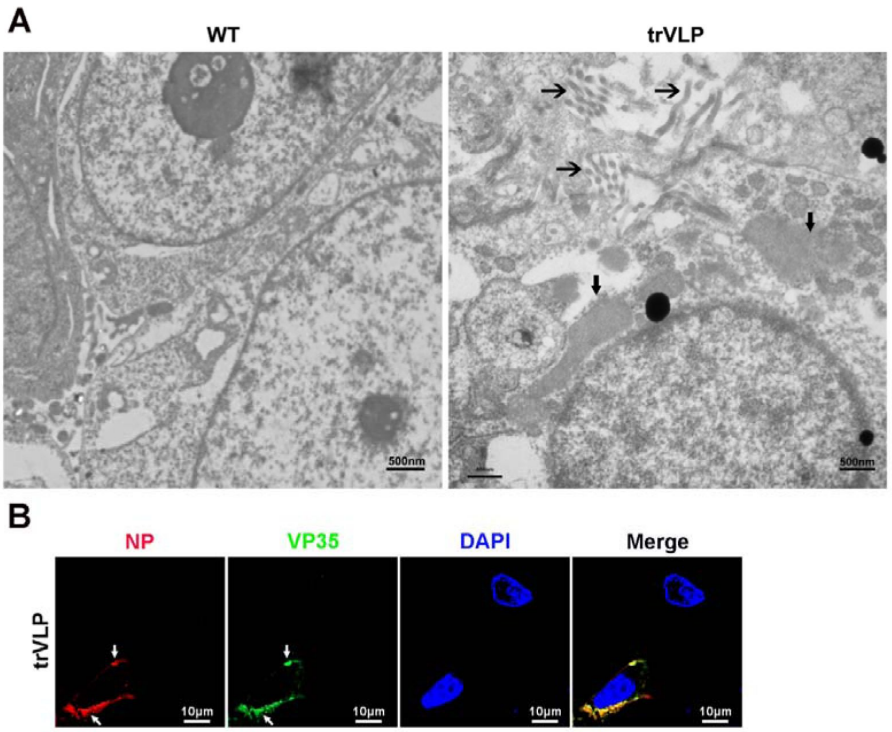

Fig. 1– figure supplement 1.

Transmission electron microscopy and immunofluorescence detection of EBOV trVLPs and IBs.

(A), HepG2 cells transfected with or without EBOV trVLP (p0) were fixed and observed with a HITACHI H-7650 transmission electron microscope at an accelerating voltage of 80 kV. The IBs and viral particles (right panel) are marked with bold arrows and regular arrows, respectively. Scale bar, 500 nm. (B), HepG2 cells transfected with the EBOV minigenome (p0) were immunostained with anti-NP (red) and anti-VP35 (green) antibodies. Nuclei were stained with DAPI (blue), and images were obtained using a Zeiss LSM 800 Meta confocal microscope. Scale bar, 10 μm.

IBs sequestration of IRF3 was further investigated at different hours post infection (hpi) of EBOV trVLPs. Detectable IRF3 puncta colocalized with viral proteins were apparent at 36 hpi in infected cells and correlated significantly with the size and shape of the viral IBs (Fig. 2A and 2B). As the size of IBs increased at 48 hpi, nearly all IRF3 colocalized with viral IBs, whereas the IRF3 distribution was completely different in the uninfected cells nearby (Fig. 2A and 2B). Using a fluorophore line of interest analysis, we assessed the intensity profiles of cytoplasmic IRF3 intensity in IBs as well as the increase in the diameter of the aggregates (Fig. 2C). As infection proceeded, the intensity of the IRF3 signal in the puncta increased as the level of cytoplasmic-dispersed IRF3 decreased (Fig. 2A), indicating that the total amount of IRF3 in the cells did not dramatically change during infection (Fig. 2D) and that only its subcellular localization changed. Taken together, the results above showed that IRF3, but not TBK1 or IKKε, was sequestered in viral IBs.

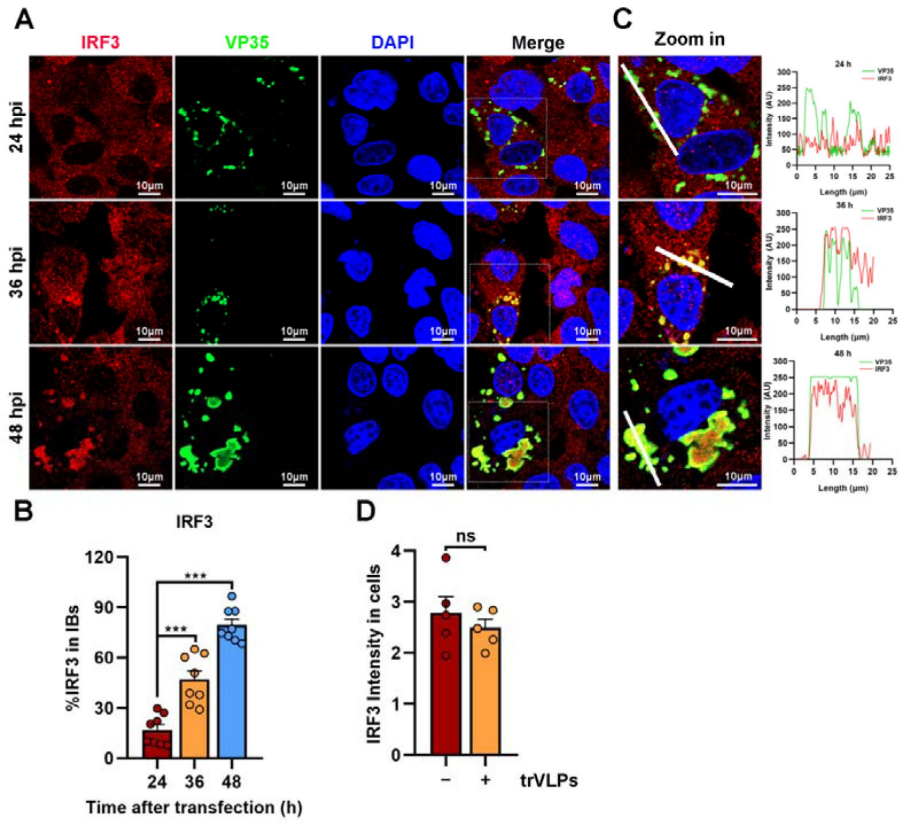

Fig. 2

EBOV trVLP induced the recruitment of IRF3 into intracytoplasmic IBs.

(A), HepG2 cells were transfected with the EBOV minigenome (p0). At the indicated time points posttransfection, cells were fixed and immunostained with anti-IRF3 (red) and anti-VP35 (green) antibodies. Nuclei were stained with DAPI (blue), and images were obtained using a Zeiss LSM 800 Meta confocal microscope. Scale bar, 10 μm. The data from two independent replicates are presented. (B), The percentage of IRF3 distribution in IBs at different time points in cells infected with EBOV trVLPs (A) was analyzed with R programming language. The intensity of IRF3 in 8 cells from two independent assays is presented as the mean ± SEM (n=8; ***$P < 0.001$). (C), The left panel shows a magnified image of the IBs boxed in the merged panel of (A). The graphs (right panel) show fluorescent intensity profiles along the indicated white lines drawn across one or more IBs. (D), The IRF3 intensity in cells infected with or without EBOV trVLPs for 48 h (the lower panel of (A)) was analyzed by ImageJ software. Differences between the two groups were evaluated using a two-sided unpaired Student's *t*-test. The intensity of IRF3 in 5 cells from two independent assays is presented as the mean ± SEM (n=5; ns, not significant).

EBOV trVLPs infection attenuates the TBK1-IRF3 association and IRF3 nuclear translocation

Upon virus infection, IRF3, as a critical transcription factor in the IFN induction pathway, can be phosphorylated and activated by TBK1, and then phosphorylated IRF3 translocates from the cytoplasm into the nucleus, eliciting the expression of antiviral IFNs. Given the sequestration of IRF3 by EBOV trVLPs in IBs, the TBK1-IRF3 association in EBOV trVLPs-infected cells was accessed by an *in situ* Duolink proximity ligation assay (PLA). Cytoplasmic complexes consisting of endogenous TBK1 with IRF3 (the red signal) were observed in HepG2 cells treated with poly(I:C), which induces the activation of the RIG-I signal cascade and IRF3 phosphorylation, and poly(I:C)-induced TBK1: IRF3 complexes were significantly reduced by EBOV trVLPs infection (Fig. 3A and 3B). Decreased TBK1-IRF3 association was further demonstrated by immunoprecipitation (Fig. 3C). Moreover, as shown in Fig. 3D, SeV infection-induced IRF3 phosphorylation and nuclear translocation were significantly inhibited by EBOV trVLPs (Fig. 3D, 4A and 4B). Importantly, IRF3 was also recruited into IBs-like compartments in the cytoplasm in the cells infected with live EBOV (Fig. 4C). These data collectively suggested that the EBOV-mediated sequestration of IRF3 in IBs blocks IRF3

phosphorylation and nuclear translocation in the TBK1-IRF3 signaling cascade, which is critical for IFN induction.

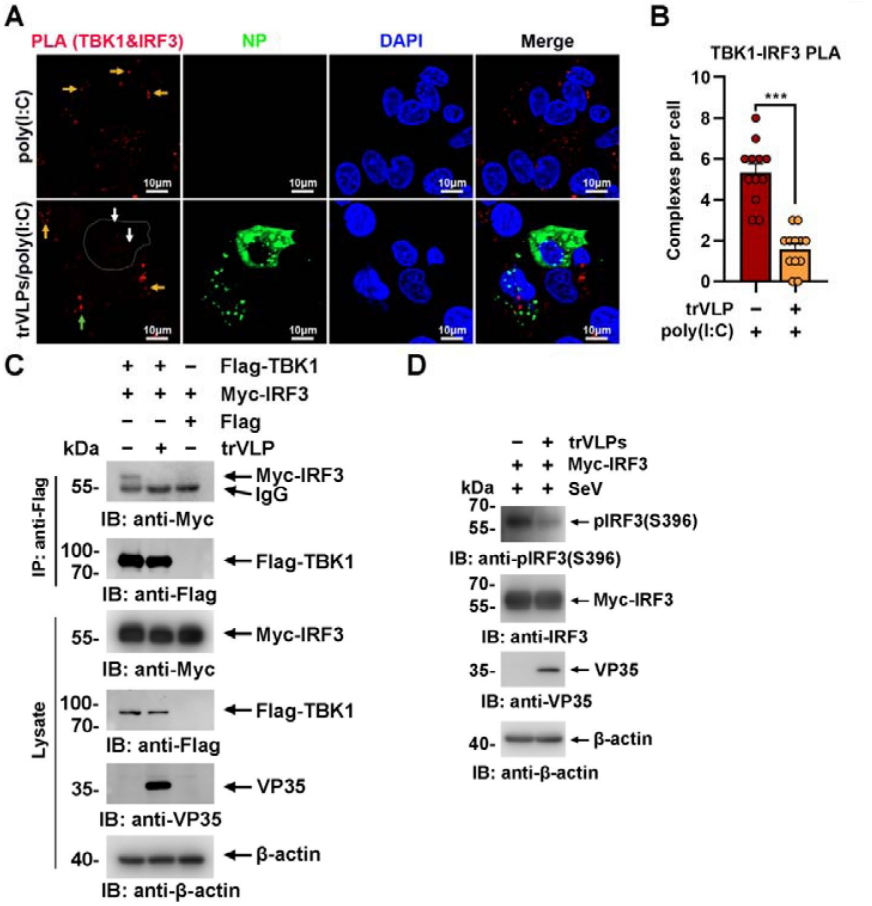

Fig. 3

EBOV trVLPs inhibited IRF3 activation.

(A), HepG2 cells were transfected with or without the EBOV minigenome (p0). Thirty-six hours after transfection, the cells were treated with or without 5 μg/ml poly(I:C) for 12 h and then subjected to *in situ* PLA with anti-TBK1 and anti-IRF3 antibodies and immunostaining with an anti-NP antibody (green). Nuclei were stained with DAPI (blue), and images were obtained using a Zeiss LSM 800 Meta confocal microscope. Arrows: white arrows represent TBK1-IRF3 complexes in trVLPs-infected cells, and yellow and green arrows represent TBK1-IRF3 complexes in uninfected and infected cells with small IBs, respectively. Scale bar, 10 μm. (B), The signal for the PLA complex in each cell in (A) was counted from at least 12 cells and is presented as the mean ± SEM. (C), Lysates of HEK293 cells cotransfected with or without the EBOV minigenome (p0) and the indicated plasmids were subjected to anti-Flag immunoprecipitation and analyzed by immunoblotting. (D), HEK293 cells were cotransfected with or without the EBOV minigenome (p0) and Myc-IRF3 plasmids. Thirty-six hours after transfection, the cells were infected with SeV at an MOI of 2 for 12 h, and the phosphorylation of IRF3 was analyzed by immunoblotting with an anti-IRF3-S396 antibody.

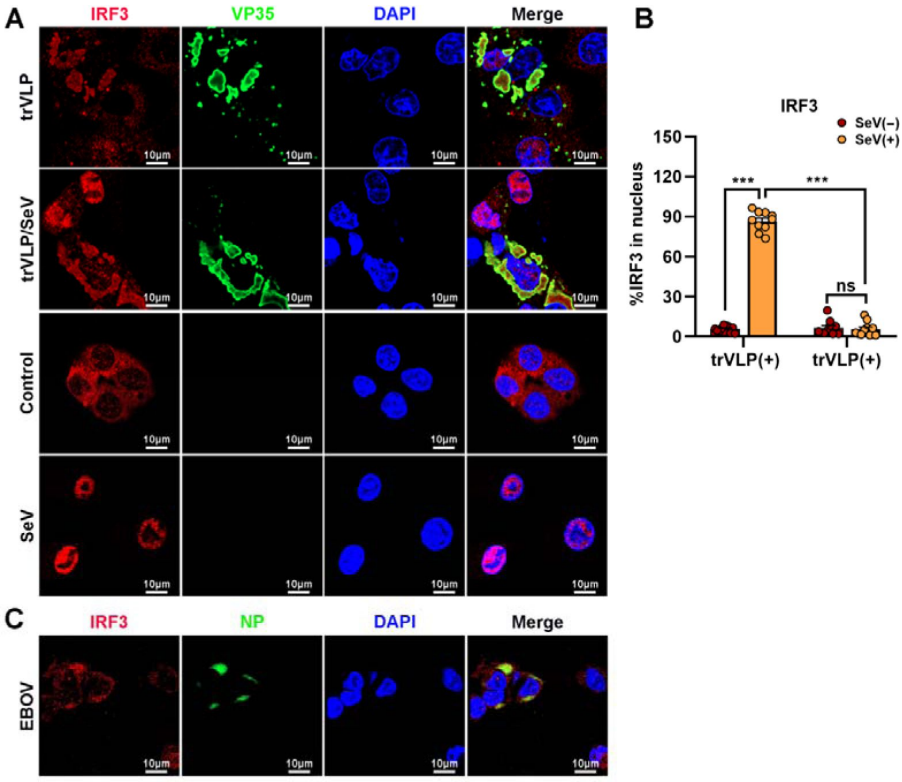

Fig. 4

EBOV trVLPs inhibited nuclear translocation of IRF3.

(A), HepG2 cells were cotransfected with or without the EBOV minigenome (p0) for 36 h, and the cells were infected with or without SeV at an MOI of 2 for another 12 h. Then, the cells were fixed and immunostained with anti-IRF3 (red) and anti-VP35 (green) antibodies. Nuclei were stained with DAPI (blue), and images were obtained using a Zeiss LSM 800 Meta confocal microscope. Scale bar, 10 μm. (B), The percentage of IRF3 nuclear distribution in (A) was analyzed by ImageJ software. The ratio of IRF3 distribution in ten cells from two independent assays is presented as the mean ± SEM (ns, not significant, ***$P < 0.001$). (C), HepG2 cells infected with live EBOV (MOI=10) for 72 h were immunostained with anti-IRF3 (red) and anti-NP (green) antibodies. Nuclei were stained with DAPI (blue), and images were obtained using a Zeiss LSM 800 Meta confocal microscope. Scale bar, 10 μm.

IBs-like structures formed by the viral proteins VP35 and NP play a key role in inducing IRF3 sequestration

Ectopic expression of NP alone (Noda, Watanabe, Sagara, & Kawaoka, 2007) or NP and the VP35 protein (Noda, Kolesnikova, Becker, & Kawaoka, 2011) in cells was sufficient to form IBs-like structures. To investigate the viral protein(s) involved in the sequestration of IRF3 in IBs, HepG2 cells were transiently transfected with plasmids encoding NP/VP35, NP/VP35/L, NP/VP35/L/VP30, NP/VP35/L/VP30/VP24, or NP/VP35/L/VP30/vRNA-RLuc/T7 and stained with anti-IRF3 and anti-NP at 48 hpi. Coexpression of NP and VP35 resulted in substantial sequestration of IRF3 in the IBs-like structure, which in turn resulted in a significant reduction of IRF3 in the nucleus, as observed in the cells transfected with vectors only and treated with poly(I:C) (Fig. 5A and 5B). Little if any VP35 or NP was demonstrated to interact with IRF3 by immunoprecipitation (Fig. 5 – figure supplement 1A-B). Compared to NP/VP35 coexpression, the presence of protein L, VP30 and VP24 showed little, if any, effect on IBs-like structure formation, IRF3 sequestration and nuclear IRF3 levels (Fig. 5A and 5B). These results suggested that IBs-like structures as well as VP35 expression were indispensable for IRF3 sequestration.

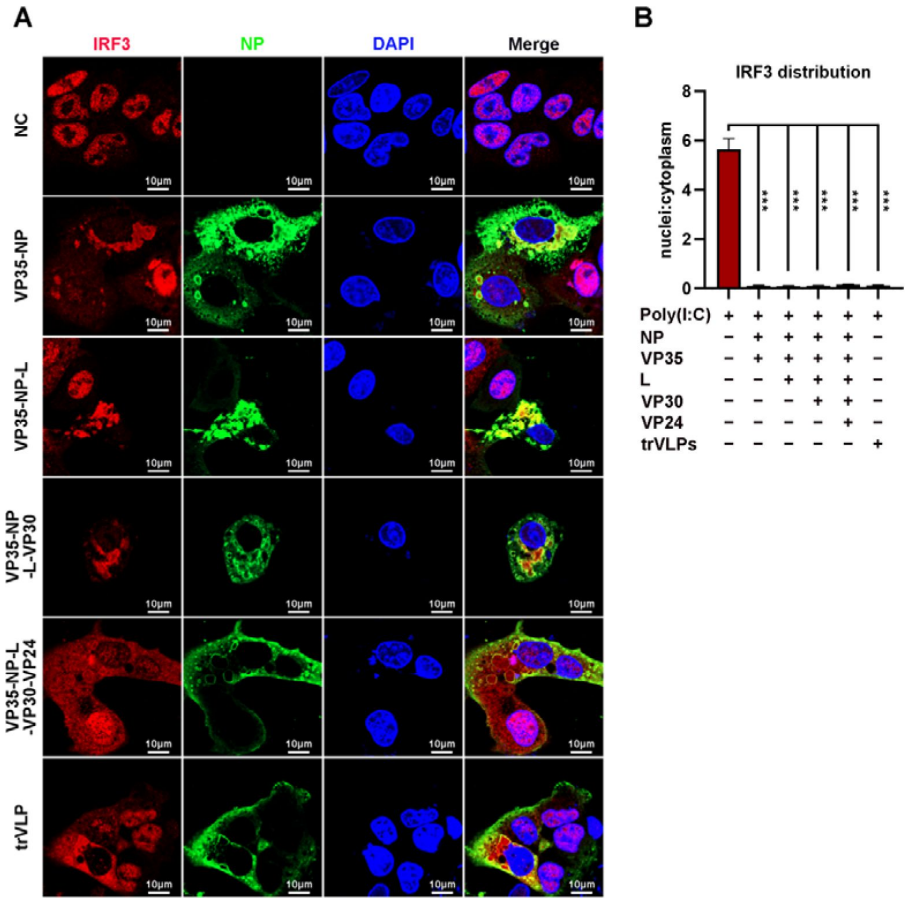

Fig. 5

EBOV NP and VP35 play an important role in sequestering IRF3 into IBs.

(A), HepG2 cells were transfected with the indicated plasmids for 36 h, and the cells were treated with 5 μg/ml poly(I:C) for another 12 h. Then, the cells were fixed and immunostained with anti-IRF3 (red) and anti-NP (green) antibodies. Nuclei were stained with DAPI (blue), and images were obtained using a Zeiss LSM 800 Meta confocal microscope. Scale bar, 10 μm. (B), The nuclear/cytoplasmic distribution of IRF3 in (A) was analyzed by ImageJ software. Differences between the two groups were evaluated using a two-sided unpaired Student's *t*-test. The ratio of IRF3 distribution in at least 5 cells from two independent assays is presented as the mean ± SEM (n=5; ***P* < 0.01, ****P* < 0.001).

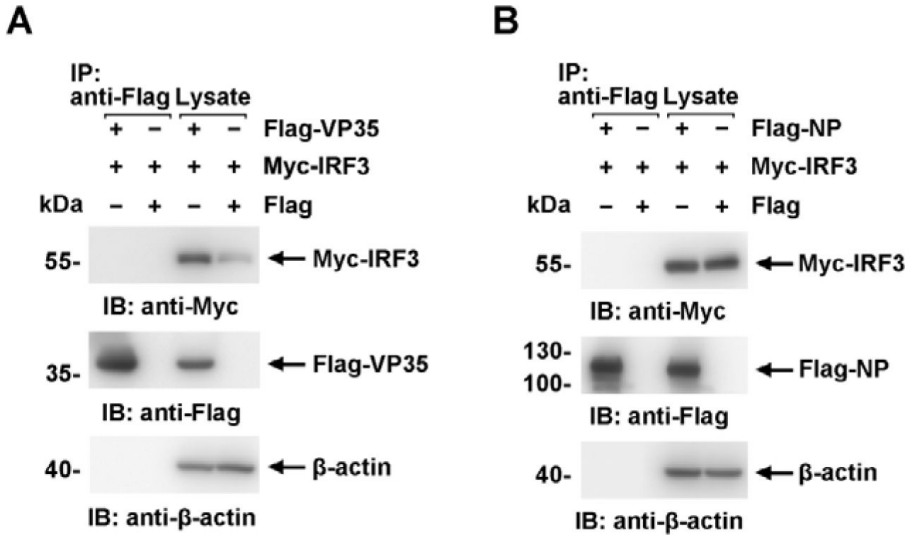

Fig. 5– figure supplement 1.

Neither VP35 nor NP interacts directly with IRF3 in cells.

(A and B) Lysates of HEK293 cells transfected with the indicated plasmids were subjected to anti-Flag immunoprecipitation and analyzed by immunoblotting. The data from two independent replicates are presented.

VP35: STING interactions play an important role in isolating IRF3 into viral IBs

TBK1 and IKKε were spatially separated from VP35 upon infection by EBOV trVLPs (Fig. 1B and 1C), and IRF3 itself was demonstrated not to interact with VP35 (Fig. 5 – figure supplement 1A-B), implying that other IRF3-interacting proteins might be involved in IRF3 sequestration in IBs upon viral infection. Stimulator of IFN genes (STING), an endoplasmic reticulum adaptor associated with IRF3 (Petrasek et al., 2013), was observed to interact with VP35 (Fig. 6A) and be recruited into IBs when the cells were infected by EBOV trVLPs (Fig. 6B and 6C). A substantial portion of STING was found to be recruited into IBs at 36 hpi in EBOV trVLPs-infected cells (Fig. 6D, 6E and Fig. 6 – figure supplement 1). STING knockdown by siRNA inhibited IRF3 sequestration in viral IBs (Fig. 6F and 6G). These results suggested that STING played important roles in the sequestration of IRF3 in viral IBs, possibly by interacting with VP35.

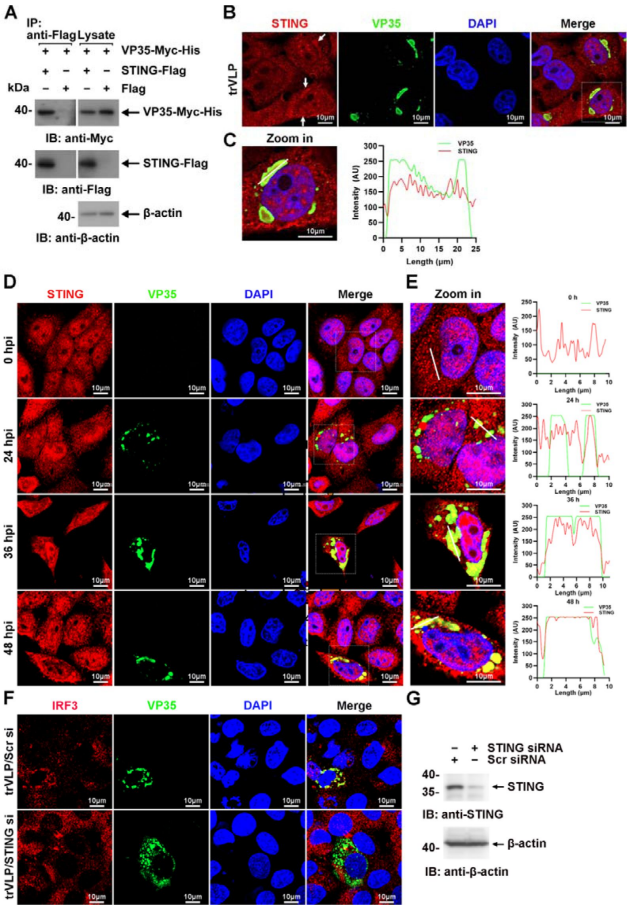

Fig. 6

EBOV trVLP recruit IRF3 into viral IBs via STING.

(A), Lysates of HEK293 cells transfected with the indicated plasmids were subjected to anti-Flag immunoprecipitation and analyzed by immunoblotting. (B) HepG2 cells were transfected with the EBOV minigenome (p0). Forty-eight hours after infection, the cells were fixed and immunostained with anti-STING (red) and anti-VP35 (green) antibodies. White arrows: STING in IBs. Nuclei were stained with DAPI (blue), and images were obtained using a Zeiss LSM 800 Meta confocal microscope. Scale bar, 10 μm. (C) The left panel shows a magnified image of the IBs boxed in the merged panel of (B). The graphs (right panel) show fluorescent intensity profiles along the indicated white lines drawn across one or more IBs. (D) HepG2 cells were transfected with the EBOV minigenome (p0). At the indicated time points post-transfection, cells were fixed and immunostained with anti-STING (red) and anti-VP35 (green) antibodies. Nuclei were stained with DAPI (blue), and images were obtained using a Zeiss LSM 800 Meta confocal microscope. Scale bar, 10 μm. The data from two independent replicates are presented. (E) The left panel shows a magnified image of the IBs boxed in the merged panel of (D). The graphs (right panel) show fluorescent intensity profiles along the indicated white lines drawn across one or more IBs. (F and G) HepG2 cells were transfected with STING siRNA (STING si) or scrambled siRNA (Scr si) for 6 h. Next, the cells were transfected with the EBOV minigenome (p0) for 36 h and then immunostained with anti-VP35 (green) and anti-IRF3 (red) antibodies. The silencing efficiency of the STING siRNA was determined by immunoblotting (G).

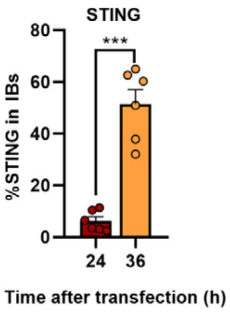

Fig. 6– figure supplement 1.

EBOV trVLP recruit STING into viral IBs.

The percentage of STING distribution in IBs at different time points in cells infected with EBOV trVLPs in Fig. 6D was analyzed with R programming language. The intensity of STING in 6 cells from two independent assays is presented as the mean ± SEM (n=6; ***P < 0.001).

Viral IBs-induced IRF3 sequestration suppresses IFN-β production

EBOV trVLPs could hijack IRF3 and sequester IRF3 into IBs and thus block the nuclear translocation of IRF3, which suggested that EBOV trVLPs may suppress IRF3-driven IFN-β production. As reported previously (Basler et al., 2000), expression of VP35 (Fig. 7A), but not NP, resulted in a mild inhibition of SeV-induced IFN-β-Luc expression (Fig. 7B). Coexpression of VP35 and NP, which led to the formation of IBs and the sequestration of IRF3 (Fig. 5A), suppressed IFN-β-Luc expression much more potently than VP35 expression alone (Fig. 7B). Coexpression of NP/VP35/L/VP30 was more potent in the inhibition of SeV-induced IFN-β-Luc expression than NP/VP35 (Fig. 7B). Moreover, coexpression of NP/VP35/VP30/L almost completely suppressed poly(I:C)-induced IFN-β transcription (Fig. 7C). *IRF3* depletion showed little, if any, effect on IFN-β transcription upon NP/VP35/L/VP30 coexpression (Fig. 7C), which suggested that NP/VP35/L/VP30 coexpression was similarly powerful as *IRF3* depletion in antagonizing IFN-β expression. These results strongly suggested that viral IBs sequestration of IRF3 was substantially more powerful than that of VP35 expression.

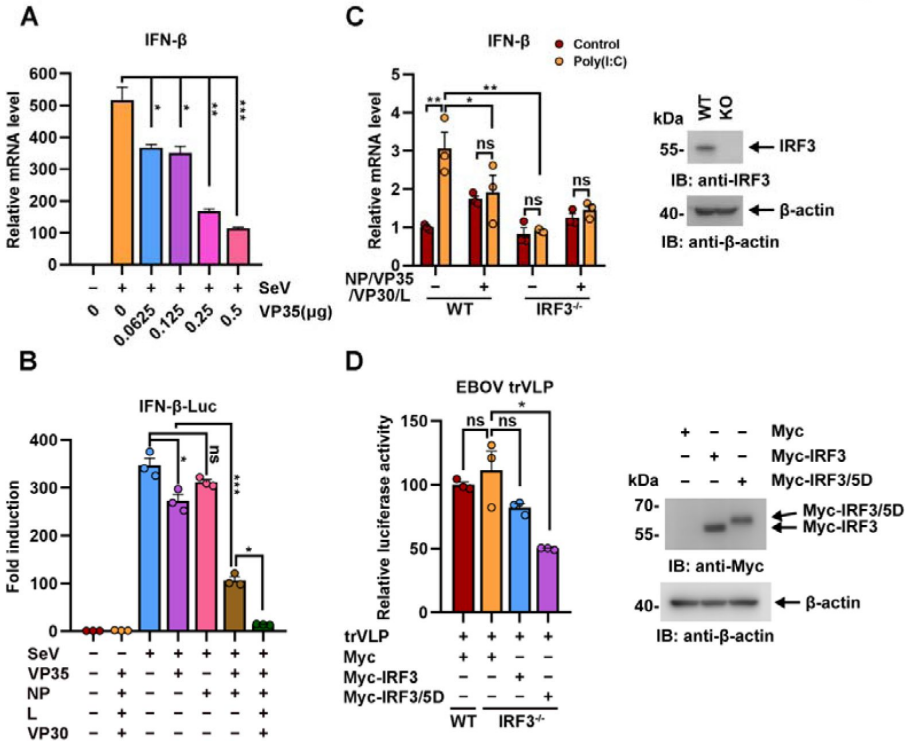

Fig. 7

IRF3 hijacked by viral IBs inhibits IFN-β production.

(A), HEK293 cells were transfected with the indicated plasmids for 24 h, and the cells were infected with or without SeV at an MOI of 2 for another 12 h. The mRNA level of IFN-β was quantified using qRT-PCR. Differences between the two groups were evaluated using the two-sided unpaired Student's *t*-test. Data are presented as the mean ± SEM (*P < 0.05, **P < 0.01, ***P < 0.001). (B), HEK293 cells were cotransfected with the firefly luciferase reporter plasmid pGL3-IFN-β-Luc, the *Renilla* luciferase control plasmid pRL-TK, and viral protein expression plasmids (0.0625 μg pCAGGS-NP, 0.0625 μg pCAGGS-VP35, 0.0375 μg pCAGGS-VP30 and

0.5 μg pCAGGS-L) for 24 h, and the cells were infected with or without SeV at an MOI of 2 for another 12 h. Then, luciferase activities were analyzed. The data were analyzed for fold induction by normalizing the firefly luciferase activity to the *Renilla* luciferase activity. Empty plasmid without SeV infection was used as a control, and the corresponding data point was set to 100%. Differences between the two groups were evaluated using the two-sided unpaired Student's *t*-test. Data are presented as the mean ± SEM (ns, not significant, **P* < 0.05, ****P* < 0.001). (C), Wild-type (WT) and *IRF3*-depleted ($IRF3^{-/-}$) HeLa cells were transfected with or without pCASSG-NP, pCASSG-VP35, pCASSG-VP30 and pCASSG-L plasmids for 36 h and then treated with or without 5 μg/ml poly(I:C) for 12 h. The mRNA level of IFN-β was quantified using qRT-PCR (left panel). Differences between the two groups were evaluated using the two-sided unpaired Student's *t*-test. Data are presented as the mean ± SEM (ns, not significant, **P* < 0.05). Lysates of WT and $IRF3^{-/-}$ HeLa cells were analyzed by immunoblotting with an anti-IRF3 antibody (right panel). (D), Wild-type (WT) and *IRF3* knockout ($IRF3^{-/-}$) HeLa cells were transfected with the EBOV minigenome (p0), pGL3-promoter and Myc-vector, Myc-IRF3 or Myc-IRF3/5D plasmids for 96 h. The amounts of trVLPs were determined by luciferase activity assay (left panel). Differences between the two groups were evaluated using the two-sided unpaired Student's *t*-test. Data are presented as the mean ± SEM (ns, not significant, ****P* < 0.001). Lysates of WT and $IRF3^{-/-}$ HeLa cells transfected with Myc-vector, Myc-IRF3 or Myc-IRF3/5D were analyzed by immunoblotting with the indicated antibodies (right panel).

We next assessed the effect of IRF3 hijacking and sequestration by viral IBs on EBOV trVLPs replication. Compared with wild-type cells, *IRF3* depletion showed little, if any, effect on EBOV replication, as indicated by luciferase activity, suggesting that trVLPs efficiently blocked IRF3 signaling (Fig. 7D). Moreover, overexpression of IRF3/5D (a phospho-mimic of activated IRF3), but not IRF3, inhibited EBOV trVLPs replication in *IRF3*-depleted cells (Fig. 7D). Taken together, these results suggest that the hijacking of IRF3 and sequestration into IBs by EBOV trVLPs can be significantly more potent in the inhibition of IFN-I production, thereby antagonizing the inhibitory effect of IFN-I on viral replication.

Discussion

Accumulating evidence suggests that EBOV has established multiple ways to antagonize host innate immune responses to maintain viral replication. Several EBOV proteins (VP35, VP24, GP, VP30 and VP40) are known to participate in host immune evasion to facilitate viral replication and pathogenesis (Audet & Kobinger, 2015; Bhattacharyya, 2021; Cantoni & Rossman, 2018). VP35 was demonstrated to suppress IFN-I production by inhibiting IRF3/7 phosphorylation, disrupting DC maturation, and facilitating the escape of immune sensation by dsRNA (Basler, 2015; Cardenas et al., 2006; Messaoudi, Amarasinghe, & Basler, 2015; Prins et al., 2009). VP30 and VP40 suppress RNA silencing by interacting with Dicer and modulating RNA interference components via exosomes, respectively (Fabozzi, Nabel, Dolan, & Sullivan, 2011; Pleet, DeMarino, Lepene, Aman, & Kashanchi, 2017). VP24 and GP are also known to block IFN-I signaling by hiding MHC-1 on the cell surface and counteracting tetherin or interfering with established immune responses by adsorbing antibodies against GP, respectively (Audet & Kobinger, 2015; Bhattacharyya, 2021).

Viral IBs are a characteristic of cellular EBOV infection and are important sites for viral RNA replication, and NP and VP35 are extremely critical proteins for the formation of IBs structures (Hoenen et al., 2012). However, whether viral IBs are involved in antagonizing IFN-I production during EBOV trVLPs infection has not yet been reported. Here, we found that IRF3 is hijacked and sequestered into EBOV IBs by viral infection (Fig. 1A), which demonstrates that viral IBs are utilized for IRF3 compartmentalization. Meanwhile, this compartmentalization resulted in the spatial isolation of IRF3 from the kinases TBK1 and

IKKε (Fig. 1B and 1C). This suggests that IRF3 deprivation by viral IBs may antagonize host antiviral signaling by inhibiting IFN-I production signaling.

As expected, the expression of NP/VP35/VP30/L, which is involved in the composition of IBs, was significantly more antagonistic to SeV-induced IFN-β production than the expression of VP35 alone (Fig. 7B). In addition, the expression of NP/VP35/VP30/L can significantly antagonize the promoting effect of poly(I:C) on IFN-β transcription, and IRF3 knockout could not further inhibit the transcription of IFN-β (Fig. 7C), which may be because viral hijacking of IRF3 into IBs nearly completely antagonized its function of promoting IFN-β production. Furthermore, knockout of IRF3 in cells cannot further promote EBOV trVLPs replication compared to wild-type cells (Fig. 7D), which may be because IRF3 is hijacked into viral IBs and cannot be phosphorylated into the nucleus to regulate IFN-I production. These results suggest that viral IBs act as virus-built 'jails' to imprison transcription factors and present a novel and possible common mechanism of viral immune evasion in which the critical signaling molecule IRF3 is spatially segregated from the antiviral kinases TBK1 and IKKε.

Although almost all IRF3 could be sequestered to viral IBs formed by VP35 and NP (Fig. 5A and 5B), we found that neither VP35 nor NP interacted with IRF3 (Fig. 5 – figure supplement 1). Here, we found that VP35 interacts with STING and colocalizes in IBs and that knockdown of STING inhibits the sequestration of IRF3 in IBs (Fig. 6A-G). These results suggest that VP35 may hijack IRF3 into IBs through STING. However, whether other host proteins are involved in this process and the role of NP in the recruitment of IRF3 by VP35 remains unclear. In addition, we found that VP35 may hijack IRF3 into IBs via STING association (Fig. 6A-6C); however, whether VP35 activates the STING-IRF3 pathway in a cGAS-independent manner by interacting with STING and the molecular mechanism remain to be further investigated.

In summary, EBOV VP35 sequesters IRF3 into viral IBs and inhibits the association of IRF3 with TBK1 and IKKε, preventing IRF3 from entering the nucleus and thereby inhibiting IFN-I production (Fig. 8). Therefore, this study reveals a new strategy by which EBOV escapes the innate immune response and provides new ideas for Ebola virus disease treatment.

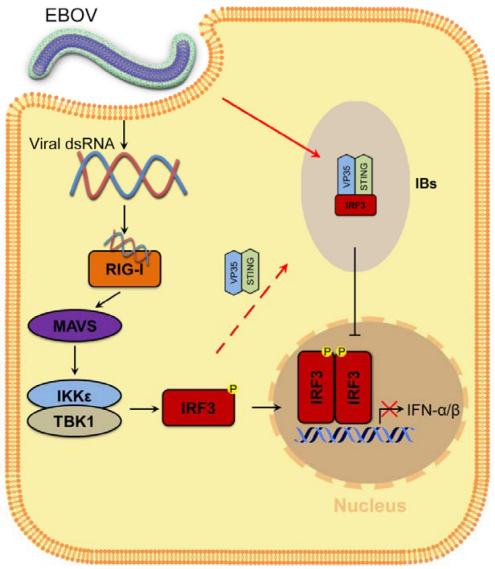

Fig. 8

Model of the molecular mechanism by which EBOV hijacks IRF3 into viral IBs through VP35-STING to comprehensively disrupt IFN-I production.

VP35 sequesters IRF3 to EBOV IBs, which in turn spatially segregates IRF3 from TBK1 and IKKε, blocks RLR signaling and inhibits IFN-I production.

Materials and Methods

Cell lines and transfections

HEK293, HeLa and IRF3-knockout HeLa cells (ABclonal, RM02113) were grown in Dulbecco's modified Eagle's medium (DMEM, Gibco). HepG2 cells were grown in minimum essential medium (MEM, Gibco) supplemented with a 1% nonessential amino acid solution (NEAA, Gibco). All media were supplemented with 10% heat-inactivated fetal bovine serum (Gibco), 2 mM L-glutamine, 100 units/ml penicillin and 100 units/ml streptomycin, and cells were grown at 37°C under an atmosphere with 5% CO_2. Transient transfection was performed with Lipofectamine 3000 (Invitrogen) according to the manufacturer's instructions.

Vectors and viruses

Flag-tagged VP35, NP, STING, TBK1 and IRF3 vectors were constructed by cloning the corresponding gene fragments into a pcDNA3.0-based Flag-vector (Invitrogen). Myc-tagged VP35, IRF3 and IRF3/5D vectors were constructed by inserting the corresponding gene fragments into the pCMV-Myc vector (Clontech). All the constructs were validated by Sanger DNA sequencing.

SeV was amplified in 9- to 11-day embryonated specific pathogen-free (SPF) eggs. Live EBOV (Mayinga strain) is preserved by the BSL-4 Lab at the Wuhan Institute of Virology, Chinese Academy of Sciences.

Immunoprecipitation and immunoblot analysis

Cell lysates were prepared in lysis buffer containing 1% Nonidet P-40 and protease inhibitor cocktail (Roche) (Cao, Leng, & Kufe, 2003). Soluble proteins were immunoprecipitated using anti-Flag (M2, Sigma), anti-Myc (Sigma) or IgG of the same isotype from the same species as a negative control (Sigma). An aliquot of the total lysate (5%, v/v) was included as a control. Immunoblotting was performed with horseradish peroxidase (HRP)-conjugated anti-Myc (Sigma), HRP-conjugated anti-Flag (Sigma), HRP-conjugated anti-β-actin (Sigma), anti-VP35 (Creative Diagnostics), anti-IRF3 (Cell Signaling Technology), anti-STING (Proteintech) or anti-NP (Sino Biological) antibodies. The antigen-antibody complexes were visualized via chemiluminescence (Immobilon Western Chemiluminescent HRP Substrate, Millipore). A PageRuler Western marker (Thermo) was used as a molecular weight standard.

Gene silencing using siRNA

For gene knockdown in HepG2 cells, cells maintained in 6-well plates were transfected with 100 pmol STING small interfering RNA (siRNA) (sense, 5'- GCACCUGUGUCCUGGAGUATT -3'; antisense, 5'- UACUCCAGGACACAGGUGCTT -3') or the same concentration of scrambled siRNA (sense, 5'- UUCUCCGAACGUGUCACGUTT -3'; antisense, 5'- ACGUGACACGUUCGGAGAATT -3') purchased from Tsingke Biotechnology (Beijing, China) with Lipofectamine 3000 (Invitrogen) according to the manufacturer's recommendations.

Reverse transcription and quantitative RT-PCR

Total cellular RNA was prepared using an RNeasy Mini kit (QIAgen, USA) according to the manufacturer's protocol. For cDNA synthesis, 0.5 μg of RNA was first digested with gDNA Eraser to remove contaminated DNA and then reverse transcribed using ReverTra Ace qPCR

RT Master Mix with gDNA Remover (FSQ-301, Toyobo) in a 20 μL reaction volume. Then, 1 μL of cDNA was used as a template for quantitative PCR. The following primers were used in these experiments: h-IFN-β F: 5'-AGGACAGGATGAACTTTGAC-3' h-IFN-β R: 5'-TGATAGACATTAGCCAGGAG-3' h-GAPDH F: 5'-AAggTCATCCCTgAgCTgAAC-3' h-GAPDH R: 5'-ACgCCTgCTTCACCACCTTCT-3'

The samples were denatured at 95°C for 2 min, followed by 40 cycles of amplification (15 s at 94°C for denaturation, 60 s at 60°C for annealing and extension). Quantitative RT-PCR (qRT-PCR) was performed using SYBR Green Real-time PCR Master Mix (QPK-201, Toyobo) with the QuantStudio 6 Flex multicolor real-time PCR detection system (ABI). Relative mRNA levels were normalized to GAPDH levels and calculated using the $2^{-\Delta\Delta CT}$ method (Livak & Schmittgen, 2001). The means (upper limit of the box) ± SEM (error bars) of three independent experiments are presented in the figures.

In situ proximity ligation assay

Duolink *in situ* PLA (Sigma) was used to detect the endogenous association of IRF3 and TBK1 in cells. In brief, HepG2 cells plated on glass coverslips were transfected with EBOV minigenome plasmids. After fixation with 4% formaldehyde, the cells were permeabilized with 0.3% Triton X-100 in PBS for 15 min. After blocking with blocking buffer (Sigma, DUO82007), the cells were incubated with mouse anti-IRF3 (Cell Signaling Technology) and rabbit anti-TBK1 (Abcam) primary antibodies. The nuclei were stained with DAPI (blue). The red fluorescent spots generated from the DNA amplification-based reporter system combined with oligonucleotide-labeled secondary antibodies were detected with a Zeiss LSM 800 Meta confocal microscope (Carl Zeiss).

Immunofluorescence microscopy

Cells were transfected, fixed, permeabilized and blocked as described above. Then, after incubation with anti-TBK1 (Cell Signaling Technology), anti-IKKε (Cell Signaling Technology), anti-IRF3 (Cell Signaling Technology), anti-VP35 (Creative Diagnostics), anti-NP (Sino Biological) or anti-STING (Bioss) antibodies overnight at 4°C, the cells were washed three times with blocking solution and then incubated with FITC- or TRITC-conjugated goat anti-rabbit (or anti-mouse) IgG. The cells were then stained with DAPI after washing and imaged using a laser scanning confocal microscope (Zeiss LSM 800 Meta) with a 63× oil immersion lens.

Luciferase reporter assay

The IFN-I production assay was performed as described previously (Zhu et al., 2022). Briefly, HEK293 cells (1×10^5 cells per well in a 24-well plate) were cotransfected with the indicated amount of pCAGGS-NP (75 ng)/pCAGGS-VP35 (75 ng)/pCAGGS-VP30 (37.5 ng)/pCAGGS-L (500 ng), 200 ng of the IFN-β reporter plasmid (Promega, USA) and 4 ng of *Renilla* luciferase plasmid. An empty vector was used to ensure that each well contained the same plasmid concentration. After 24 h, the cells were treated with SeV (MOI=2) or 5 μg/ml poly(I:C) for 12 h, and the luciferase activity of the cell lysates was analyzed with the dual-luciferase reporter assay system (Promega, E1960) using a GloMax 20/20 luminometer (Promega, USA). Values were obtained by normalizing the luciferase values to the Renilla values. Fold induction was determined by setting the results from the group transfected with vector without Flag-VP35 to a value of 1.

EBOV trVLPs assay

The replication of EBOV in the cells was evaluated with the minigenome system (Hoenen et al., 2014). Briefly, producer cells (p0) were cotransfected with p4cis-vRNA-RLuc (250 ng) and pCAGGS-T7 (250 ng) for T7 RNA polymerase expression and 4 plasmids for EBOV protein expression (pCAGGS-NP (125 ng), pCAGGS-VP35 (125 ng), pCAGGS-VP30 (75 ng), and pCAGGS-L (1,000 ng)), as well as the luciferase reporter vector pGL3-Promoter (Youbio, 25 ng). One day after transfection, the medium was replaced with medium containing 5% FBS, and the cells were then incubated for another 3 days. Viral replication was determined by intracellular luciferase activities using a dual-luciferase reporter assay kit (Promega, E1960) after cell lysis with passive lysis buffer (PLB, Promega). For immunofluorescence experiments, cells were harvested 48 h after transfection.

Transmission electron microscopy (TEM)

HepG2 cells transfected with EBOV minigenome p0-related plasmids were washed with PBS, fixed with 2.5% glutaraldehyde, and then prestained with osmium tetroxide. Eighty-nanometer-thick serial sections were then cut and stained with uranyl acetate and lead citrate. Images were acquired with a transmission electron microscope (Hitachi, H-7650) operating at 80 kV.

EBOV infection assay

WT HepG2 cells grown in 12-well plates were incubated with the EBOV Mayinga strain at an MOI of 10 as determined by virus titration in Vero E6 cells at 37°C for 1 h for microscopy. Then, the cells were washed 3 times with PBS, and fresh medium was added to the cells, which were incubated at 37°C for 72 h. Subsequently, the cells were fixed with 4% formaldehyde for immunofluorescence microscopy as required by the BSL-4 laboratory. All work with live EBOV was performed with BSL-4 containment.

Statistical analyses

Graphical representation and statistical analyses were performed using Prism 8 software (GraphPad Software). Unless indicated otherwise, the results are presented as the means (upper limit of the box) ± SEM (error bars) from three independent experiments conducted in duplicate. An unpaired two-tailed *t*-test was used for the analysis of two groups. Data were considered significant when $P < 0.05$ (*), $P < 0.01$ (**), and $P < 0.001$ (***).

Data availability

All the data shown in this paper are available from the corresponding authors upon reasonable request.

Acknowledgements

This work was supported by the Advanced Customer Cultivation Project of Wuhan National Biosafety Laboratory, Chinese Academy of Sciences [2022ACCP-MS04] and the National Major Science and Technology Projects of China [2018ZX09711003-005-005 to T.G., 2022YFC2600704 to H.L.].

Competing Interests statement

The authors declare no competing interests.

Author Contributions

L.Z., X.L., and C.C. designed and supervised the study. L.Z., J.J., and T.W. performed the experiments. T.G., H.L., Q.D., Y.H., Y. J., Z.L, and P. L. analyzed the data. L.Z, X.L., and C.C. wrote the manuscript. All authors have read and approved the article.

References

Audet J. , Kobinger G. P (2015) **Immune evasion in ebolavirus infections** *Viral Immunol* **28**:10–18
https://doi.org/10.1089/vim.2014.0066

Basler C. F (2015) **Innate immune evasion by filoviruses** *Virology* **479**:122–130
https://doi.org/10.1016/j.virol.2015.03.030

Basler C. F. , Mikulasova A. , Martinez-Sobrido L. , Paragas J. , Muhlberger E. , Bray M. , Klenk H. D. , Palese P. , Garcia-Sastre A (2003) **The Ebola Virus VP35 Protein Inhibits Activation of Interferon Regulatory Factor 3** *J Virol* **77**:7945–7956
https://doi.org/10.1128/jvi.77.14.7945-7956.2003

Basler C. F. , Wang X. , Muhlberger E. , Volchkov V. , Paragas J. , Klenk H. D. , Garcia-Sastre A. , Palese P (2000) **The Ebola virus VP35 protein functions as a type I IFN antagonist** *P Natl Acad Sci Usa* **97**:12289–12294
https://doi.org/10.1073/pnas.220398297

Bhattacharyya S (2021) **Mechanisms of Immune Evasion by Ebola Virus** *Adv Exp Med Biol* **1313**:15–22
https://doi.org/10.1007/978-3-030-67452-6_2

Cantoni D. , Rossman J. S (2018) **Ebolaviruses: New roles for old proteins** *PLoS Negl Trop Dis* **12**
https://doi.org/10.1371/journal.pntd.0006349

Cao C. , Leng Y. , Kufe D (2003) **Catalase activity is regulated by c-Abl and Arg in the oxidative stress response** *J Biol Chem* **278**:29667–29675
https://doi.org/10.1074/jbc.M301292200

Cardenas W. B. , Loo Y. M. , Gale M. , Hartman A. L. , Kimberlin C. R. , Martinez-Sobrido L. , Saphire E. O. , Basler C. F (2006) **Ebola virus VP35 protein binds double-stranded RNA and inhibits alpha/beta interferon production induced by RIG-I signaling** *J Virol* **80**:5168–5178
https://doi.org/10.1128/JVI.02199-05

Fabozzi G. , Nabel C. S. , Dolan M. A. , Sullivan N. J (2011) **Ebolavirus proteins suppress the effects of small interfering RNA by direct interaction with the mammalian RNA interference pathway** *J Virol* **85**:2512–2523
https://doi.org/10.1128/JVI.01160-10

Feldmann H. , Jones S. , Klenk H. D. , Schnittler H. J (2003) **Ebola virus: from discovery to vaccine** *Nat Rev Immunol* **3**:677–685

Fitzgerald K. A. , McWhirter S. M. , Faia K. L. , Rowe D. C. , Latz E. , Golenbock D. T. , Coyle A. J. , Liao S. M. , Maniatis T (2003) **IKKepsilon and TBK1 are essential components of the IRF3 signaling pathway** *Nat Immunol* **4**:491–496
https://doi.org/10.1038/ni921

Haasnoot J. , de Vries W. , Geutjes E. J. , Prins M. , de Haan P. , Berkhout B. (2007) **The Ebola virus VP35 protein is a suppressor of RNA silencing** *Plos Pathog* **3**:794–803
https://doi.org/10.1371/journal.ppat.0030086

Hoenen T. , Shabman R. S. , Groseth A. , Herwig A. , Weber M. , Schudt G. , Dolnik O. , Basler C. F. , Becker S. , Feldmann H (2012) **Inclusion Bodies Are a Site of Ebolavirus Replication** *J Virol* **86**:11779–11788
https://doi.org/10.1128/jvi.01525-12

Hoenen T. , Watt A. , Mora A. , Feldmann H (2014) **Modeling the lifecycle of Ebola virus under biosafety level 2 conditions with virus-like particles containing tetracistronic minigenomes** *Jove-J Vis Exp* **91**
https://doi.org/10.3791/52381

Hong Y. , Bai M. , Qi X. , Li C. , Liang M. , Li D. , Cardona C. J. , Xing Z (2019) **Suppression of the IFN-alpha and -beta Induction through Sequestering IRF7 into Viral Inclusion Bodies by Nonstructural Protein NSs in Severe Fever with Thrombocytopenia Syndrome Bunyavirus Infection** *J Immunol* **202**:841–856
https://doi.org/10.4049/jimmunol.1800576

Lee J. K. , Shin O. S (2021) **Nonstructural Protein of Severe Fever with Thrombocytopenia Syndrome Phlebovirus Inhibits TBK1 to Evade Interferon-Mediated Response** *J Microbiol Biotechnol* **31**:226–232
https://doi.org/10.4014/jmb.2008.08048

Liu S. , Cai X. , Wu J. , Cong Q. , Chen X. , Li T. , Du F. , Ren J. , Wu Y. T. , Grishin N. V. , Chen Z. J (2015) **Phosphorylation of innate immune adaptor proteins MAVS, STING, and TRIF induces IRF3 activation** *Science* **347**
https://doi.org/10.1126/science.aaa2630

Livak K. J. , Schmittgen T. D (2001) **Analysis of relative gene expression data using real-time quantitative PCR and the 2(-Delta Delta C(T)) Method** *Methods* **25**:402–408
https://doi.org/10.1006/meth.2001.1262

Mahanty Siddhartha , Bray Mike (2004) **Pathogenesis of filoviral haemorrhagic fevers** *Lancet Infect Dis* **4**:487–498
https://doi.org/10.1016/s1473-3099(04)01103-x

McCarthy S. D. , Majchrzak-Kita B. , Racine T. , Kozlowski H. N. , Baker D. P. , Hoenen T. , Kobinger G. P. , Fish E. N. , Branch D. R (2016) **A Rapid Screening Assay Identifies Monotherapy with Interferon-ss and Combination Therapies with Nucleoside Analogs as Effective Inhibitors of Ebola Virus** *PLoS Negl Trop Dis* **10**
https://doi.org/10.1371/journal.pntd.0004364

Messaoudi Ilhem , Amarasinghe Gaya K. , Basler Christopher F (2015) **Filovirus pathogenesis and immune evasion: insights from Ebola virus and Marburg virus** *Nat Rev Microbiol* **13**:663–676
https://doi.org/10.1038/nrmicro3524

Misasi J. , Sullivan N. J (2014) **Camouflage and misdirection: the full-on assault of Ebola virus disease** *Cell* **159**:477–486
https://doi.org/10.1016/j.cell.2014.10.006

Nanbo Asuka , Watanabe Shinji , Halfmann Peter , Kawaoka Yoshihiro (2013) **The spatio-temporal distribution dynamics of Ebola virus proteins and RNA in infected cells** *Sci Rep* **3**
https://doi.org/10.1038/srep01206

Ning Y. J. , Feng K. , Min Y. Q. , Cao W. C. , Wang M. , Deng F. , Hu Z. , Wang H (2015) **Disruption of type I interferon signaling by the nonstructural protein of severe fever with thrombocytopenia syndrome virus via the hijacking of STAT2 and STAT1 into inclusion bodies** *J Virol* **89**:4227–4236
https://doi.org/10.1128/JVI.00154-15

Ning Y. J. , Wang M. , Deng M. , Shen S. , Liu W. , Cao W. C. , Deng F. , Wang Y. Y. , Hu Z. , Wang H (2014) **Viral suppression of innate immunity via spatial isolation of TBK1/IKKepsilon from mitochondrial antiviral platform** *J Mol Cell Biol* **6**:324–337
https://doi.org/10.1093/jmcb/mju015

Noda T. , Kolesnikova L. , Becker S. , Kawaoka Y (2011) **The importance of the NP: VP35 ratio in Ebola virus nucleocapsid formation** *J Infect Dis* **204**:S878–883
https://doi.org/10.1093/infdis/jir310

Noda T. , Watanabe S. , Sagara H. , Kawaoka Y (2007) **Mapping of the VP40-binding regions of the nucleoprotein of Ebola virus** *J Virol* **81**:3554–3562
https://doi.org/10.1128/JVI.02183-06

Petrasek J. , Iracheta-Vellve A. , Csak T. , Satishchandran A. , Kodys K. , Kurt-Jones E. A. , Fitzgerald K. A. , Szabo G (2013) **STING-IRF3 pathway links endoplasmic reticulum stress with hepatocyte apoptosis in early alcoholic liver disease** *P Natl Acad Sci Usa* **110**:16544–16549
https://doi.org/10.1073/pnas.1308331110

Pleet M. L. , DeMarino C. , Lepene B. , Aman M. J. , Kashanchi F (2017) **The Role of Exosomal VP40 in Ebola Virus Disease** *DNA Cell Biol* **36**:243–248
https://doi.org/10.1089/dna.2017.3639

Prins K. C. , Cardenas W. B. , Basler C. F (2009) **Ebola virus protein VP35 impairs the function of interferon regulatory factor-activating kinases IKKε and TBK-1** *J Virol* **83**:3069–3077
https://doi.org/10.1128/JVI.01875-08

Reid S. P. , Cardenas W. B. , Basler C. F (2005) **Homo-oligomerization facilitates the interferon-antagonist activity of the ebolavirus VP35 protein** *Virology* **341**:179–189
https://doi.org/10.1016/j.virol.2005.06.044

Reid S. P. , Leung L. W. , Hartman A. L. , Martinez O. , Shaw M. L. , Carbonnelle C. , Volchkov V. E. , Nichol S. T. , Basler C. F (2006) **Ebola virus VP24 binds karyopherin alpha1 and blocks STAT1 nuclear accumulation** *J Virol* **80**:5156–5167
https://doi.org/10.1128/JVI.02349-05

van Tol S. , Kalveram B. , Ilinykh P. A. , Ronk A. , Huang K. , Aguilera-Aguirre L. , Bharaj P. , Hage A. , Atkins C. , Giraldo M. I. , Wakamiya M. , Gonzalez-Orozco M. , Warren A. N. , Bukreyev A. , Freiberg A. N. , Rajsbaum R. (2022) **Ubiquitination of Ebola virus VP35 at lysine 309 regulates viral transcription and assembly** *PLoS Pathog* **18**
https://doi.org/10.1371/journal.ppat.1010532

Wu X. , Qi X. , Qu B. , Zhang Z. , Liang M. , Li C. , Cardona C. J. , Li D. , Xing Z (2014) **Evasion of antiviral immunity through sequestering of TBK1/IKKepsilon/IRF3 into viral inclusion bodies** *J Virol* **88**:3067–3076
https://doi.org/10.1128/JVI.03510-13

Yen B. , Mulder L. C. , Martinez O. , Basler C. F (2014) **Molecular basis for Ebolavirus VP35 suppression of human dendritic cell maturation** *J Virol* **88**:12500–12510
https://doi.org/10.1128/JVI.02163-14

Zhu Lin , Gao Ting , Huang Yi , Jin Jing , Wang Di , Zhang Leike , Jin Yanwen , Li Ping , Hu Yong , Wu Yan , Liu Hainan , Dong Qincai , Wang Guangfei , Zheng Tong , Song Caiwei , Bai Yu , Zhang Xun , Liu Yaoning , Yang Weihong , Xu Ke , Zou Gang , Zhao Lei , Cao Ruiyuan , Zhong Wu , Xia Xianzhu , Xiao Gengfu , Liu Xuan , Cao Cheng (2022) **Ebola virus VP35 hijacks the PKA-CREB1 pathway for replication and pathogenesis by AKIP1 association** *Nat Commun* **13**
https://doi.org/10.1038/s41467-022-29948-4

Zhu Lin , Gao Ting , Yang Weihong , Liu Yaoning , Liu Xuan , Hu Yong , Jin Yanwen , Li Ping , Xu Ke , Zou Gang , Zhao Lei , Cao Ruiyuan , Zhong Wu , Xia Xianzhu , Cao Cheng (2020) **Ebola virus replication is regulated by the phosphorylation of viral protein VP35** *Biochem Bioph Res Co* **521**:687–692
https://doi.org/10.1016/j.bbrc.2019.10.147

Author information

Lin Zhu
Institute of Biotechnology, Academy of Military Medical Sciences, Beijing, 100850, China

Jing Jin
Institute of Physical Science and Information Technology, Anhui University, Hefei, Anhui 230601, China

Tingting Wang
Institute of Physical Science and Information Technology, Anhui University, Hefei, Anhui 230601, China

Yong Hu
Institute of Biotechnology, Academy of Military Medical Sciences, Beijing, 100850, China

Hainan Liu
Institute of Biotechnology, Academy of Military Medical Sciences, Beijing, 100850, China

Ting Gao
Institute of Biotechnology, Academy of Military Medical Sciences, Beijing, 100850, China

Qincai Dong
Institute of Biotechnology, Academy of Military Medical Sciences, Beijing, 100850, China

Yanwen Jin
Institute of Biotechnology, Academy of Military Medical Sciences, Beijing, 100850, China

Ping Li
Institute of Biotechnology, Academy of Military Medical Sciences, Beijing, 100850, China

Zijing Liu
Institute of Biotechnology, Academy of Military Medical Sciences, Beijing, 100850, China

Xuan Liu
Institute of Biotechnology, Academy of Military Medical Sciences, Beijing, 100850, China
For correspondence: liux931932@163.com

Cheng Cao
Institute of Biotechnology, Academy of Military Medical Sciences, Beijing, 100850, China
For correspondence: caoc@nic.bmi.ac.cn

Editors

Reviewing Editor
Sara Sawyer
University of Colorado Boulder, United States of America

Senior Editor
Sara Sawyer
University of Colorado Boulder, United States of America

Reviewer #1 (Public Review):

The authors were trying to investigate whether viral IBs are involved in antagonizing IFN-I production during EBOV trVLPs infection. They found that IRF3 is hijacked and sequestered into EBOV IBs after viral infection, thereby leading to the spatial isolation of IRF3 with TBK1 and IKKε. In such a progress, the activity of IRF3 is suppressed and downstream IFN-I induction is inhibited. The authors designed many experiments, such as the PLA that examined the colocalization, to support their conclusions. However, necessary negative controls were missed in several assays. More key index is needed to be examined in several assays.

The paper is well organized and most data in this paper could support the conclusions, while there are several issues that need to be further solved.

1. In Figure 2-4, authors should examine the expression of downstream IFNs as well as the phosphorylation and nuclear localization of IRF3 to further prove the suppression of IRF3 activity by infecting with trVLPs.

2. In Figure 5, to better prove the conclusion that EBOV NP and VP35 play an important role in sequestering IRF3 in IBS, authors should add the "NP+VP35+VP30" and "NP+VP35+VP24" groups to reperform the assay.

3. In Figure 6f, the expression of STING should be examined by immunostaining to show the knockdown efficiency in trVLPs-infected cells.

Reviewer #2 (Public Review):

The manuscript by Zhu et al explored molecular mechanisms by which Ebola virus (EBOV) evades host innate immune response. EBOV has a number of means to shut down the type I interferon induction (by viral VP35 protein) and block type I interferon action (by viral VP24 protein). This study reported a new mechanism that inclusion body (IB) used for viral replication sequesters IRF3, a key transcription factor involved in the interferon signaling, resulting in blockade of downstream type I interferon gene transcription. This finding is potentially interesting and may provide a new insight into EBOV's evasion of innate immunity. However, there are some flaws in the experimentations and analyses that need to be addressed.

1. Most of experiments were performed by transfection of trVLP plasmids, which is very different from virus infection. The conclusions should be examined and verified in the context of virus infection.

2. Fig 1 - VP35 displayed a classical IB staining only in Panel A, while much less so in Panel C and not in panel B. It seemed that the VP35 staining images were chosen in a way towards the authors' favor. The statistical analysis of co-localization of VP35 and IRF3, TBK1 or IKKe should be performed to draw the conclusion. Another concern is that IKKe is normally lowly expressed under a rest condition and becomes induced only when the interferon signaling is activated. It seemed to be expressed at a high level even when the interferon signaling is blocked in Panel C. The authors should comment on this discrepancy.

3. Fig 2 - Was this experiment done by transfection or infection? The description of result is not consistent with the figure legend. The labeling was also not consistent

between panel A and B. I would suggest performing Western blot to analyze the expression level of IRF3.

4. Fig 3 and 4 - As VP35 is well known for its highly efficient blockade of type I interferon activation, how would the authors differentiate the effect of VP35 alone from the sequestration of IRF3 in IBs in these experiments?

5. Fig 3 - PolyIC can activate both RLR and TLR signaling pathways. Can the author comment on which pathway it activates in this experiment?

6. The authors demonstrated that VP35 interacts with STING and recruit the latter to IBs. How would this affect the function of STING given that STING plays essential roles in cGAS/cGAMP pathway?

7. It is difficult to follow the logics of Fig 7. The expression level of each viral protein should be determined. Ideally, a mutation in VP35 that disrupts its ability to antagonize the interferon signaling but still allows for the IB formation can be used to assess the relative contribution of IB sequestering IRF3.